

# Bluish-Green BMes<sub>2</sub>-Functionalized Pt<sup>II</sup> Complexes for High Efficiency PhOLEDs: Impact of the BMes<sub>2</sub> Location on Emission Color

Ying-Li Rao,<sup>[a]</sup> Dylan Schoenmakers,<sup>[a]</sup> Yi-Lu Chang,<sup>[b]</sup> Jia-Sheng Lu,<sup>[a]</sup>  
Zheng-Hong Lu,<sup>[b]</sup> Youngjin Kang,<sup>\*,[c]</sup> and Suning Wang<sup>\*,[a]</sup>

**Abstract:** New phosphorescent Pt<sup>II</sup> compounds based on dimesitylboron (BMes<sub>2</sub>)-functionalized 2-phenylpyridyl (ppy) N,C-chelate ligands and an acetylacetonato ancillary ligand have been achieved. We have found that BMes<sub>2</sub> substitution at the 4'-position of the phenyl ring can blue-shift the phosphorescent emission energy of the Pt<sup>II</sup> compound by approximately 50 nm, compared to the 5'-BMes<sub>2</sub> substituted analogue, without substantial loss of luminescent quantum efficiencies. The emission color of the 4'-BMes<sub>2</sub> substituted Pt<sup>II</sup> compound, Pt(Bppy)(acac) (**1**) can be further tuned by the introduction of a substituent group at the 3'-

position of the phenyl ring. A methyl substituent red-shifts the emission energy of **1** by approximately 10 nm whereas a fluoro substituent blue-shifts the emission energy by about 6 nm. Using this strategy, three bright blue-green phosphorescent Pt<sup>II</sup> compounds **1**, **2** and **3** with emission energy at 481, 492, and 475 nm and  $\Phi_{\text{PL}} = 0.43$ , 0.26 and 0.25, respectively, have been achieved. In addition, we have examined the impact of BMes<sub>2</sub> substitution on 3,5-dipyridylbenzene (dpb) N,C,N-che-

late Pt<sup>II</sup> compounds by synthesizing compound **4**, Pt(Bdppb)Cl, which has a BMes<sub>2</sub> group at the 4'-position of the benzene ring. Compound **4** has a phosphorescent emission band at 485 nm and  $\Phi_{\text{PL}} = 0.70$ . Highly efficient blue-green electroluminescent (EL) devices with a double-layer structure and compounds **1**, **3** or **4** as the phosphorescent dopant have been fabricated. At 100 cd m<sup>-2</sup> luminance, EL devices based on **1**, **3** and **4** with an external quantum efficiency of 4.7, 6.5 and 13.4%, respectively, have been achieved.

**Keywords:** OLEDs • organoborons • platinum • synthesis • structure

## Introduction

Phosphorescent organic light-emitting diodes (PhOLEDs) have recently received much attention because of their applications in next-generation flat-panel displays and solid-state lighting devices.<sup>[1]</sup> The key challenge in PhOLEDs research is the development of phosphorescent metal complexes with high quantum efficiency, especially blue phosphorescent compounds. Much earlier and current research efforts on phosphorescent materials for OLEDs focus on 2-phenylpyridine(Hppy)-based Ir<sup>III</sup> complexes and their derivatives because of their high photoluminescent quantum efficiencies.<sup>[2]</sup> Although highly efficient PhOLEDs based on Ir<sup>III</sup>

emitters have been achieved, stable blue PhOLEDs based on Ir<sup>III</sup> compounds remain elusive.<sup>[3]</sup> Compared with Ir<sup>III</sup> complexes, Pt<sup>II</sup> compounds that have a high phosphorescent quantum efficiency are scarce due to often strong intermolecular  $\pi$ - $\pi$  stacking interactions caused by the square-planar geometry, leading to excimer formation and decrease of emission quantum efficiency and color purity in the solid state.<sup>[4]</sup> The square-planar geometry of Pt<sup>II</sup> may have one advantage over Ir<sup>III</sup>, namely the access to a higher triplet state, due to the greater ligand field splitting that greatly increases the energy of the d-d state, for a given set of chelate ligands.<sup>[5]</sup> This may be evident from the emission energy (538 nm) of Pt(BppyB)(acac) and that (605 nm) of the Ir<sup>III</sup> analogue (Scheme 1). Thus, Pt<sup>II</sup> compounds are good candidates for the development of blue phosphorescent emitters, if low emission efficiency and intermolecular interaction issues can be addressed. Several examples of green, orange or red phosphorescent Pt<sup>II</sup> compounds have been demonstrated recently for successful use in PhOLEDs,<sup>[4,6,7]</sup> blue PhOLEDs based on Pt<sup>II</sup> compounds are very rare and only a few examples are known in the literature.<sup>[8,9]</sup>

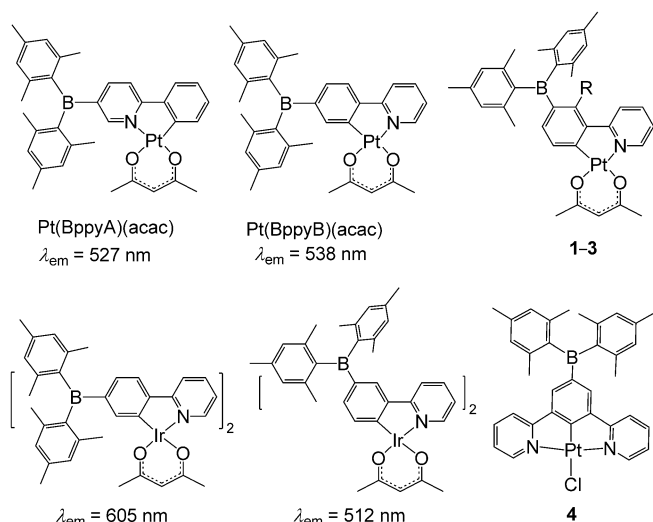
We have recently shown that high efficiency green and orange PhOLEDs with external quantum efficiency as high as 20% can be achieved by using dimesitylboron (BMes<sub>2</sub>) functionalized Pt(ppy)(acac) and derivative compounds.<sup>[7]</sup> We have shown that the introduction of the BMes<sub>2</sub> group to the N,C-chelate backbone plays several important roles in

[a] Y.-L. Rao, D. Schoenmakers, J.-S. Lu, Prof. S. Wang  
Department of Chemistry, Queen's University  
Kingston, Ontario, K7L 3N6 (Canada)  
Fax: (+1) 613 533 6669  
E-mail: wangs@chem.queensu.ca

[b] Y.-L. Chang, Prof. Z.-H. Lu  
Department of Materials Science and Engineering  
University of Toronto, Ontario, M5S 3E4 (Canada)

[c] Prof. Y. Kang  
Division of Science Education, Kangwon National University  
Chuncheon 200-701 (Republic of Korea)  
E-mail: kang@kangwon.ac.kr

Supporting information for this article is available on the WWW under <http://dx.doi.org/10.1002/chem.201201255>.



Scheme 1. Emission energies of previously synthesized phosphorescent  $\text{Pt}^{\text{II}}$  compounds and their  $\text{Ir}^{\text{III}}$  analogues, and the newly synthesized compounds **1–4**.

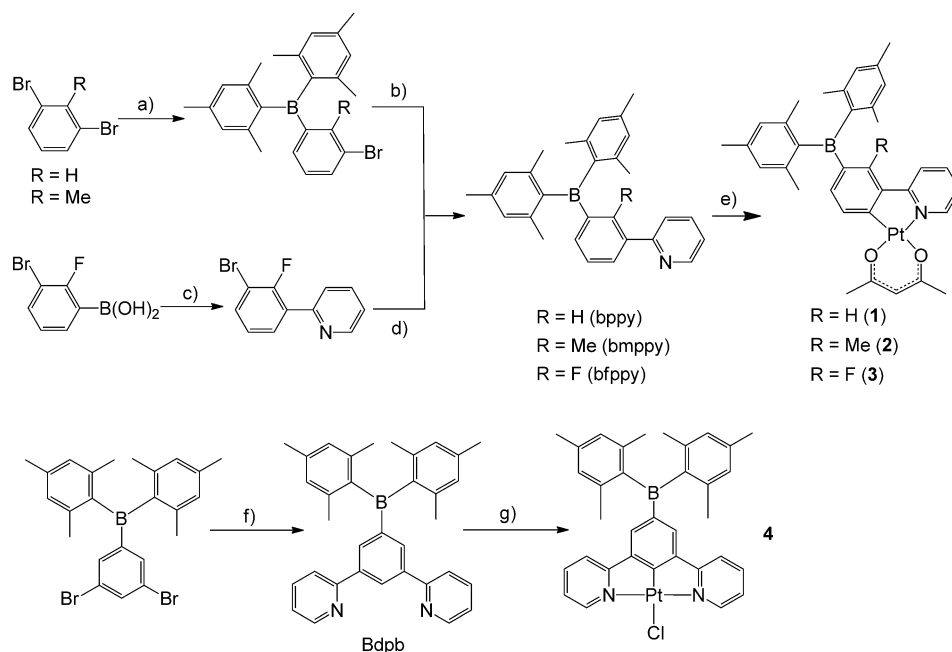
the high performance of the resulting  $\text{Pt}^{\text{II}}$  compounds in PhOLEDs. First of all, it facilitates the mixing of the  $^3\text{LC}$  and the MLCT state, thus enhancing the intrinsic phosphorescent efficiency of the molecule. Secondly, it minimizes intermolecular interactions, thus enhancing emission efficiency in the solid state. Thirdly, it facilitates electron injection into the emissive layer/dopant, thus improving the device efficiency. The excellent performance by our first generation  $\text{BMe}_2$ -functionalized N,C-chelate  $\text{Pt}^{\text{II}}$  compounds inspired us to investigate blue phosphorescent  $\text{Pt}^{\text{II}}$  compounds using the same boron-functionalization strategy.

In our earlier study of  $\text{BMe}_2$ -functionalized  $\text{Pt}(\text{ppy})(\text{acac})$  and derivative compounds, the  $\text{BMe}_2$  group was placed either at the pyridyl ring or the phenyl ring, *meta* to the Pt atom (e.g.,  $\text{Pt}(\text{BppyA})(\text{acac})$  and  $\text{Pt}(\text{BppyB})(\text{acac})$  in Scheme 1).<sup>[7]</sup> By examining two  $\text{BMe}_2$  functionalized Ir-ppy compounds (Scheme 1) reported by Park,<sup>[10]</sup> Wong and Marder et al.,<sup>[11]</sup> it is apparent that the location of the  $\text{BMe}_2$  group has a great impact on emission energy. As shown in Scheme 1, placing the  $\text{BMe}_2$  group on the phenyl ring, *trans* to the  $\text{Ir}^{\text{III}}$  atom, significantly widens the HOMO–LUMO gap

and blue-shifts the emission energy. Thus, our first strategy toward achieving blue phosphorescent  $\text{Pt}^{\text{II}}$  compounds is to change the location of the  $\text{BMe}_2$  group from the *meta* or 5'-position of the phenyl ring to the *para* or 4'-position of the phenyl in the ppy ligand. In addition, we want to further tune the emission energy by varying the R group (Scheme 1). Our second strategy in achieving blue phosphorescent  $\text{Pt}^{\text{II}}$  compounds is to study  $\text{BMe}_2$ -functionalized 3,5-dipyridylbenzene (dpb) N,C,N-chelate  $\text{Pt}^{\text{II}}$  compounds since several members of N,C,N-chelate  $\text{Pt}^{\text{II}}$  compounds have been shown previously to be very promising blue-green phosphorescent emitters for OLEDs.<sup>[8,9]</sup> Based on this consideration, a new N,C,N- $\text{Pt}^{\text{II}}$  compound **4** (Scheme 1) has been synthesized and investigated. In this report, the details of synthesis and characterization of compounds **1–4**, the impact of  $\text{BMe}_2$  substitution on emission color of ppy-based N,C-chelate  $\text{Pt}^{\text{II}}$  compounds and the performance of these new compounds in PhOLEDs are presented.

## Results and Discussion

**Synthesis and crystal structure:** The synthesis route and details for boron-functionalized phenylpyridine ligands and their corresponding  $\text{Pt}^{\text{II}}$  complexes are shown in Scheme 1. In the initial study, we have attempted syntheses of **1–3** using  $\text{PtCl}(\text{DMSO})(\text{acac})$  as a typical starting material in the presence of a base according to a procedure established by our group earlier.<sup>[7a]</sup> This reaction condition, however,



Scheme 2. Reagents and conditions: a)  $n\text{BuLi}/\text{Et}_2\text{O}$ ,  $\text{B}(\text{Mes})_2\text{F}$ ,  $-78^\circ\text{C}$ , then room temperature, overnight; b) 2-Br-pyridine,  $n\text{BuLi}$ ,  $\text{ZnCl}_2(\text{tmeda})_2$ ,  $\text{Pd}(\text{PPh}_3)_4$ , THF, reflux, overnight; c) 2-Br-pyridine,  $\text{K}_2\text{CO}_3$ , THF,  $\text{Pd}(\text{PPh}_3)_4$ ,  $70^\circ\text{C}$ , 7 h; d)  $n\text{BuLi}/\text{Et}_2\text{O}$ ,  $\text{BMe}_2\text{F}$ ,  $-78^\circ\text{C}$ , then room temperature, overnight; e)  $[\text{PtMe}_2(\text{SMe}_2)]_2$ ,  $\text{CF}_3\text{SO}_3\text{H}$ ,  $\text{Na}(\text{acac})\cdot\text{H}_2\text{O}$ , room temperature, 1 to 2 h; f) 2-( $\text{Bu}_3\text{Sn}$ )pyridine,  $\text{LiCl}$ ,  $\text{Pd}(\text{PPh}_3)_2\text{Cl}_2$ , toluene, reflux, 3 days; g)  $\text{K}_2\text{PtCl}_4$ ,  $\text{CH}_3\text{CN}/\text{H}_2\text{O}$  (3:1),  $90^\circ\text{C}$ , overnight.

did not give the desired complexes except **3** and black precipitate slowly formed as the reaction progressed. Using this method, compound **3** was obtained only in low yield. To improve the synthesis of **3** and obtain compounds **1** and **2**, a recently developed alternative method<sup>[12]</sup> was used, which involves one-pot reaction of the appropriate ligand with [PtMe<sub>2</sub>(SMe<sub>2</sub>)<sub>2</sub>], without isolation of any intermediates. Using this approach, the new Pt complexes, **1–3** were obtained in high yields (80–90%). The new method is much better than the old method since it greatly shortens reaction time, uses mild conditions and produces the desired compounds in high yields. The synthesis of the BMes<sub>2</sub>-functionalized N,C,N-chelate ligand 1-dimesitylboryl-3,5-dipyridylbenzene (Bdppb) was accomplished by Stille coupling of excess 2-(tributylstannyl)pyridine with 3,5-dibromophenyldimesitylborane by using Pd(PPh<sub>3</sub>)<sub>2</sub>Cl<sub>2</sub> as the catalyst. Compound **4** was synthesized and isolated in 94% yield from the treatment of Bdppb with K<sub>2</sub>PtCl<sub>4</sub> in a mixed solvent of CH<sub>3</sub>CN and water at 90 °C.

All compounds are stable in air and soluble in common organic solvents but not in pentane, hexane and methanol. Compounds **1–4** have been fully characterized by NMR spectroscopy, elemental analyses, and X-ray diffraction analyses.

Crystallographic data for all complexes are provided in the Supporting Information. Important bond distances and angles are shown in Table 1. The structures of compounds **1–4** are shown in Figure 1. For compound **1**, three independent molecules are located in one asymmetric unit with similar bond distances and angles. For **4**, two independent molecules are located in one asymmetric unit with similar bond distances and angles. Despite the variation of the R group in structures of **1–3**, the bond lengths and bond angles around the Pt<sup>II</sup> atoms are similar. The dihedral angle between the BC<sub>2</sub> (mesityl) plane and the phenyl ring of the ppy chelate for these three compounds are also similar (21.4°, 22.0° and 24.6° in **1**; 23.6° in **2**; and 23.7° in **3**); this indicates that the change of the R group from H atom to a methyl group does not have a significant impact on the conjugation of the BMes<sub>2</sub> group with the phenyl ring of the ppy chelate. The dihedral angles between the phenyl and the pyridyl ring of the ppy ligand are 5.9(5)°, 4.4(5)° and 3.0(5)° for **1**, 12.5(7)° for **2** and

Table 1. Selected bond lengths [Å] and angles [°] for compounds **1–4**.

Compound <b>1</b>			
Pt(1)–N(1)	1.992 (9)	Pt(1)–C(1)	1.939 (12)
Pt(1)–O(1)	2.061 (8)	Pt(1)–O(2)	2.012 (8)
C(1)–Pt(1)–O(1)	175.8 (4)	N(1)–Pt(1)–O(2)	173.9 (4)
Compound <b>2</b>			
Pt(1)–N(1)	1.990 (9)	Pt(1)–C(1)	1.970 (10)
Pt(1)–O(1)	2.015 (8)	Pt(1)–O(2)	2.102 (7)
C(1)–Pt(1)–O(2)	174.8 (4)	N(1)–Pt(1)–O(1)	174.4 (3)
Compound <b>3</b>			
Pt(1)–N(1)	1.986 (4)	Pt(1)–C(1)	1.951 (4)
Pt(1)–O(1)	1.998 (3)	Pt(1)–O(2)	2.089 (3)
C(1)–Pt(1)–O(2)	175.08 (16)	N(1)–Pt(1)–O(1)	174.53 (13)
Compound <b>4</b>			
Pt(1)–N(1)	2.024 (3)	Pt(1)–N(2)	2.037 (4)
Pt(1)–C(11)	1.905 (4)	Pt(1)–Cl(1)	2.4018 (11)
N(1)–Pt(1)–N(2)	161.10 (13)	C(11)–Pt(1)–Cl(1)	177.45 (12)

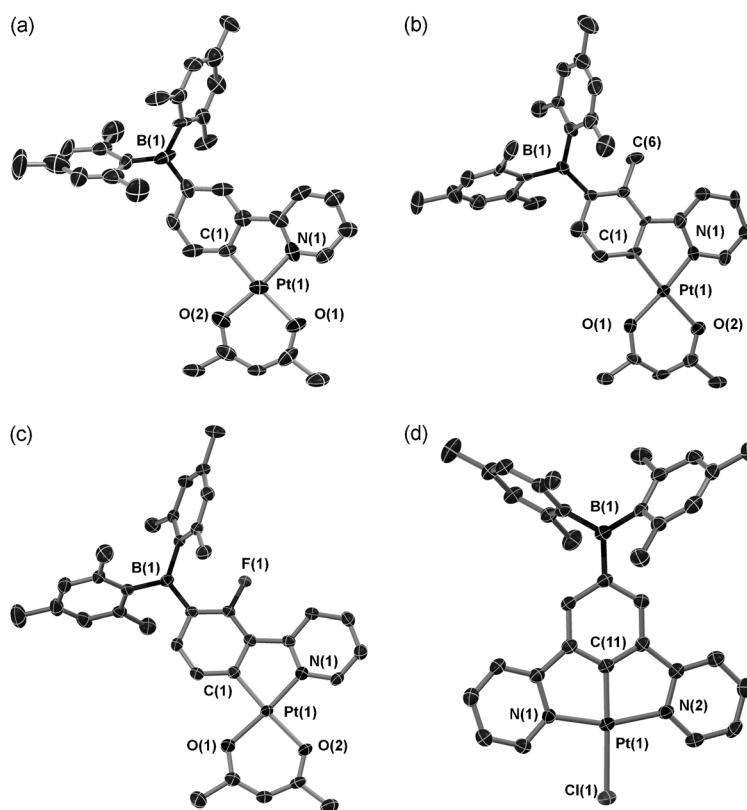


Figure 1. Structure diagrams of: a) **1**, b) **2**, c) **3**, and d) **4** with 50% thermal ellipsoids and labels of key atoms. Hydrogen atoms are omitted for clarity.

3.0(3)° for **3**, respectively. The increase of this dihedral angle from **1** to **2** is clearly caused by the steric effect of the methyl substitution in **2**. Interestingly, however, this dihedral angle for compound **3** is close to those of **1** and much less than that of **2**, which appears to be the result of strong intramolecular hydrogen bonding between fluorine and hydrogen atoms of both mesityl and pyridine ring (see the Supporting Information). These small dihedral angles prove the pres-

ence of effective  $\pi$  conjugation of the ppy chelate in all three compounds. For compounds **1–3**, the Pt–O bond *trans* to the Pt–C bond is slightly longer than that *trans* to the Pt–N bond, attributable to the greater *trans* effect exerted by the carbon atom.

Compound **1** forms a stacked dimer in the solid state with the pyridyl ring being directly above the Pt–acac chelate. The shortest Pt $\cdots$ C<sub>py</sub> separation distances in the dimer of **1** are found to be 3.64–3.67 Å and the Pt $\cdots$ Pt separation distances to be 4.64–4.67 Å (see the Supporting Information). Compound **2** also forms a similar stacked dimer with Pt $\cdots$ C<sub>py</sub> separation distance of 3.64 Å and a Pt $\cdots$ Pt separation of 4.64 Å. For **1** and **2** the stacking intermolecular interactions are limited to the discrete dimer and no extended stacking was observed in the crystal lattice. Compound **3** also forms a stacked dimer but with a much shorter Pt $\cdots$ C<sub>py</sub> separation distance (3.38 Å) and a Pt $\cdots$ Pt separation of 4.70 Å that is similar to those of **1** and **2**. Furthermore, the molecules of **3** display extended stacking with short interdimer C<sub>py</sub> $\cdots$ C<sub>py</sub> separation distance of approximately 3.26 Å and a long Pt $\cdots$ Pt separation of 6.87 Å (Figure 2). Thus, among N,C-

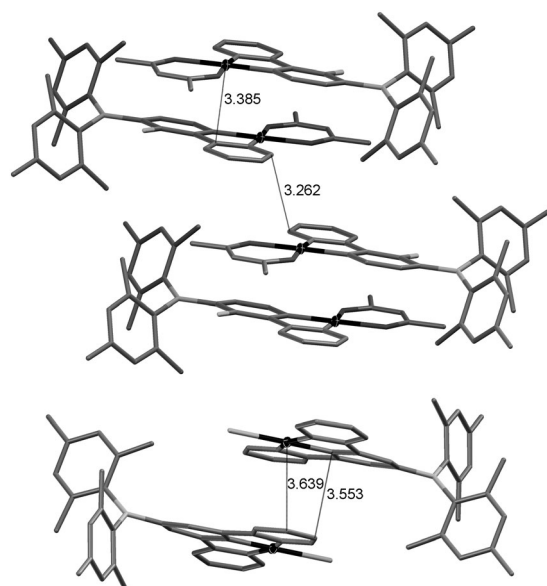


Figure 2. Diagrams showing intermolecular stacking of compound **3** (top) and **4** (bottom).

chelate compounds **1–3**, the fluoro-substituted compound is most prone to intermolecular stacking interactions. This is consistent with our earlier observation for the fluoro derivative of Pt(BppyA)(acac) that dimerizes with a short Pt $\cdots$ Pt separation distance of 3.404(1) Å.<sup>[7a]</sup> However, compared to Pt(BppyA)(acac) and Pt(BppyB)(acac) and their derivatives, which have the tendency to form dimers that stack directly along the Pt $\cdots$ Pt vector, leading to very short Pt $\cdots$ Pt separation distances and strong Pt $\cdots$ Pt interactions,<sup>[7a]</sup> none of compounds **1–3** shows similar Pt $\cdots$ Pt interactions. In fact, all intermolecular interactions in **1–3** are between the pyridyl ring and the Pt center.

The N,C,N-chelate compound **4** also forms a stacked dimer in the crystal lattice with the pyridyl ring being located directly above the Pt atom. A short interdimer Pt $\cdots$ C<sub>py</sub> separation distance of 3.64 Å and a short C $\cdots$ C separation distance of 3.55 Å between the py ring and the central phenyl ring are observed (see the Supporting Information). The Pt $\cdots$ Pt separation distance in the dimer of **4** is very long (5.70 Å) and no further extended stacking interactions are evident. The lack of direct Pt $\cdots$ Pt interactions in these new BMes<sub>2</sub>-functionalized Pt<sup>II</sup> compounds can be attributed to the presence of the bulky boron group at the 5'-position, which may inhibit the formation of excimer in either solid state or thin film.

**Thermal property:** Because small molecule-based OLEDs are fabricated by vacuum deposition at elevated temperature, it is important that the materials used in OLEDs have a high thermal stability. To investigate the impact of substitution at 4'-position of the phenyl ring on thermal properties of the new Pt<sup>II</sup> compounds, differential scanning calorimetry (DSC) diagrams were recorded for compounds **1–3**. Although none of the compounds shows glass transitions in both the first and second heating/cooling cycles, they do display a high thermal stability with a crystallization temperature at approximately 250 °C (with the order of **1** > **2** > **3**). These compounds are thermally stable up to their melting points (> 300 °C, see the Supporting Information).

**Photophysical and electrochemical properties:** Compounds **1–3** display a distinct but weak absorption band at 350–450 nm region (Figure 3), which may be attributed MLCT transitions. Compound **4** has a well resolved absorption band with a moderate intensity at 387 nm, which may be assigned to intraligand charge transfer transition. The main absorption band at approximately 330 nm for **1–3**, which is attributed to  $\pi$ – $\pi^*$  transitions of the N,C-chelate ligands, is similar to that observed in Pt(BppyB)(acac). The key difference between the new compounds **1–3** and Pt(BppyB)(acac) is the luminescence spectra. Like Pt(BppyB)(acac), compounds **1–3** are brightly luminescent with quantum efficiencies ranging from 0.43–0.26 in solution and 0.35 to 0.21 in the solid state. In contrast, the quantum efficiency of the non-borylated Pt(ppy(acac)) compound is only 0.15.<sup>[13]</sup> The phosphorescent decay lifetimes of **1–3** are also similar to that of Pt(BppyB)(acac). However, compared to Pt(BppyB)(acac), which emits at 538 nm, the emission energy of **1–3** is significantly blue-shifted with the emission maximum at 478, 485 and 470 nm, respectively (Figure 3 and Table 2). The impact of the BMes<sub>2</sub> position on the emission energy of the Pt<sup>II</sup> compounds follows the same trend as that observed for the Ir<sup>III</sup> compounds.<sup>[10,11]</sup> Furthermore, the emission colors of **1–3** do not change significantly from solution to the solid state (Table 2 and the spectra in Figure 3); this indicates that the intermolecular interactions observed in the crystal structures do not have any significant impact on luminescence of these molecules. Among compounds **1–3** the fluoro-substituted compound **3** has the shortest emission



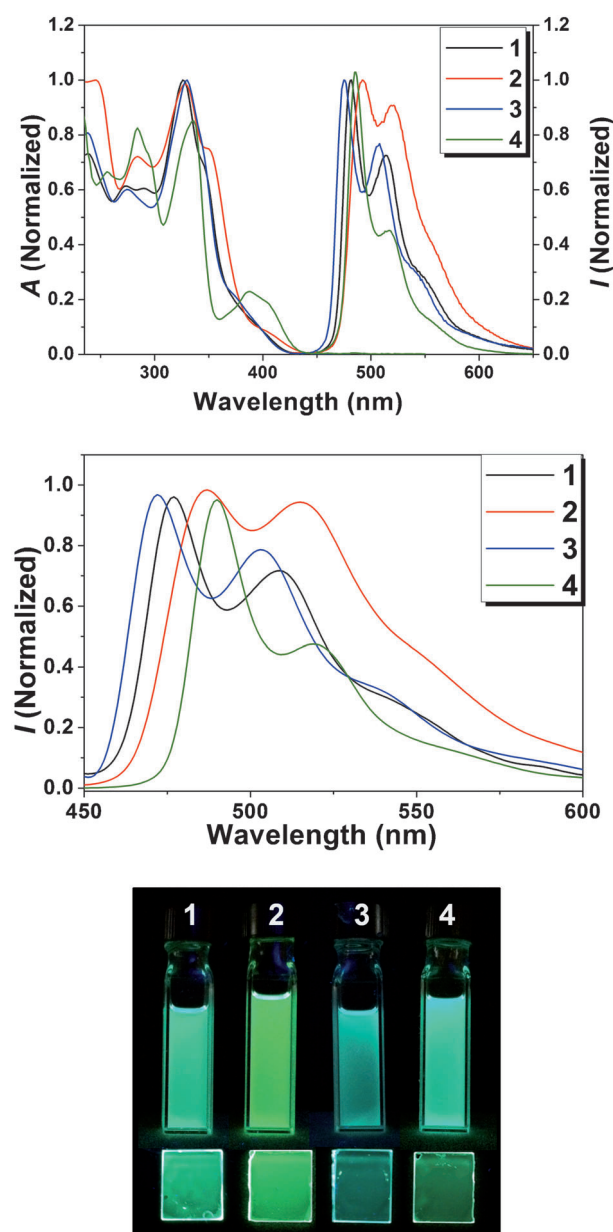


Figure 3. Top: absorption and emission spectra of **1–4** in CH<sub>2</sub>Cl<sub>2</sub> at 298 K. Middle: emission spectra of **1–4** in the solid state at 298 K (10% wt PMMA film). Bottom: photos showing the emission color of **1–4** in CH<sub>2</sub>Cl<sub>2</sub> (top) and in PMMA film (10 wt %, bottom) under 365 nm irradiation.

wavelength whereas the methyl-substituted compound **1** has the longest emission wavelength, differing by approximately 15 nm.

The emission spectrum of **4** closely resembles that of the non-borylated Pt(dpb)Cl parent molecule<sup>[9,14]</sup> (Figure 4);

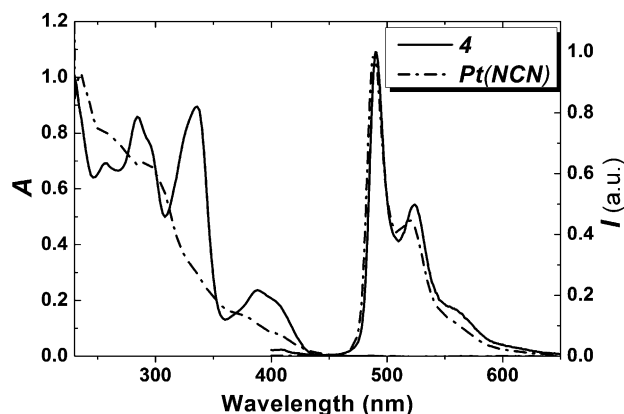


Figure 4. Absorption and emission spectra of compound **4** and Pt(dpb)Cl (Pt(NCN)) in CH<sub>2</sub>Cl<sub>2</sub>, recorded under the same conditions.

this indicates that the phosphorescence of these two molecules share a common origin, which is most likely a mixed ligand-centered  $\pi$ - $\pi^*$ , MLCT and LC transitions, as established previously for Pt(dpb)Cl.<sup>[14]</sup> Compared to Pt(dpb)Cl, the emission maximum of **4** is blue-shifted by a few nanometers with a significantly enhanced emission efficiency (0.70 in solution vs. 0.60 of Pt(dpb)Cl). Furthermore, unlike Pt(dpb)Cl, which has a very poor solubility in common organic solvents and a strong tendency to produce excimer emission in concentrated solution and the solid state due to strong intermolecular interactions,<sup>[14]</sup> the emission of **4** does not change significantly with concentration in solution or from the solution to the solid state. The bulky BMes<sub>2</sub> clearly plays a role in minimizing intermolecular interactions of **4**.

Using Equations (1) and (2), the values for the radiative ( $k_r$ ) and non-radiative ( $k_{nr}$ ) decay rates for all four new Pt<sup>II</sup> compounds were determined and compared (Figure 5). Although the  $k_r$  values are comparable to one another for **1**, **2** and **3**, the  $k_{nr}$  value of the highly emissive **4** is considerably smaller than those of **1**, **2** and **3**. Thus, the high  $\Phi_{PL}$  value

Table 2. Photophysical and electrochemical data of **1**, **2**, **3** and **4**.

Complex	Absorption <sup>[a]</sup>	Emission, 298 K, solution <sup>[a]/solid<sup>[b]</sup></sup>			Emission, 77 K <sup>[d]</sup>		$E_{1/2}^{\text{red}}$ [V] <sup>[e]</sup>
	$\lambda_{\text{max}}$ [nm], ( $\epsilon$ [ $\times 10^4 \text{ M}^{-1} \text{ cm}^{-1}$ ])	$\lambda_{\text{max}}$ [nm]	$\tau_p$ [ $\mu\text{s}$ ]	$\Phi_{\text{PL}}$ <sup>[c]</sup>	$\lambda_{\text{max}}$ [nm]	$\tau_p$ [ $\mu\text{s}$ ]	
<b>1</b>	271 (1.85), 327 (3.01), 344 (2.13)	481/476	8.7 (2)/9.5 (3)	0.43/0.35	478	9.4 (1)	−2.34
<b>2</b>	282 (2.40), 328 (3.33), 349 (2.56)	492/487	8.7 (2)/8.7 (1)	0.26/0.30	485	12.2 (2)	−2.36
<b>3</b>	274 (2.10), 331 (3.56), 343 (2.71)	475/472	9.6 (2)/7.2 (2)	0.25/0.21	470	10.2 (7)	−2.27
<b>4</b>	283 (3.10), 334 (3.20), 387 (0.87)	485/489	8.9 (2)/6.6 (2)	0.70/0.76	490	9.5 (1)	−2.09

[a] The absorption spectra were measured in degassed CH<sub>2</sub>Cl<sub>2</sub> solution; [M] =  $8.0 \times 10^{-5}$ . [b] Doped into PMMA at 10 wt %. [c] Phosphorescence quantum efficiency measured in CH<sub>2</sub>Cl<sub>2</sub>, relative to Ir(ppy)<sub>3</sub> ( $\Phi = 1.0$ ). Solid state quantum efficiency was measured by using an integration sphere (error range  $\pm 10\%$  of the reported value). [d] In frozen CH<sub>2</sub>Cl<sub>2</sub> glass. [e] The reduction potentials of all compounds were measured in DMF with NBu<sub>4</sub>PF<sub>6</sub> (0.10 M) at a scan rate of either 50 or 100 mV s<sup>−1</sup> (vs. FeCp<sub>2</sub><sup>0/+</sup>).

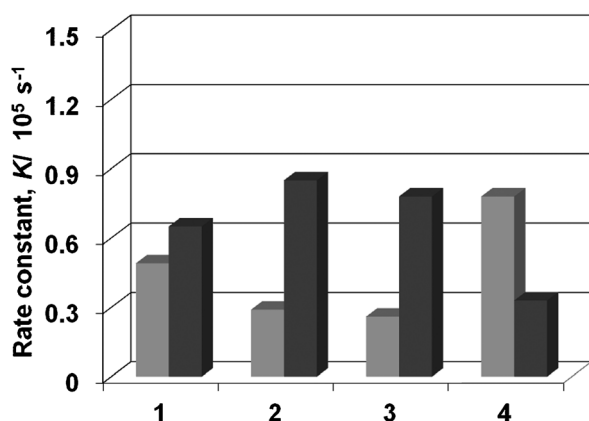


Figure 5. Radiative ( $k_r$ , ■) and non-radiative ( $k_{nr}$ , ■) rate constants for **1**, **2**, **3** and **4**.

for **4** can be attributed to the suppression of the non-radiative decay processes. Interestingly, the  $k_r$  values of **1–3** are similar with that of Pt(ppy)(acac) ( $5.7 \times 10^4 \text{ s}^{-1}$ ), whereas the  $k_{nr}$  values of **1–3** are almost five-times smaller than that of Pt(ppy)(acac) ( $3.2 \times 10^5 \text{ s}^{-1}$ ).<sup>[13,15]</sup> These results strongly indicate that the BMes<sub>2</sub> unit introduced into the ppy ligand significantly retards the non-radiative decay process, leading to improved PL efficiency.

$$\Phi_{\text{PL}} = k_r / (k_r + k_{nr}) \quad (1)$$

$$1/\tau = k_r + k_{nr} \quad (2)$$

To understand the origin of the phosphorescence blue-shift and the substitution effect observed in compounds **1–4**, electrochemical properties of these compounds were examined by cyclic voltammetry. All four compounds display a reversible reduction peak at  $E_{1/2}^{\text{red}} = -2.34, -2.36, -2.27$  for **1–3**, respectively, relative to  $\text{FcCp}_2^{+/0}$ . Using the reduction potentials and the energy of the absorption edge, HOMO and LUMO energies for compounds **1–4** were estimated (Table 3). The impact of the BMes<sub>2</sub> substitution and location can be illustrated by comparing compound **1**, Pt(BppyB)(acac) [HOMO =  $-5.45 \text{ eV}$ , LUMO =  $-2.78 \text{ eV}$ ]<sup>[7a]</sup> and Pt(ppy)(acac) [HOMO =  $-5.31 \text{ eV}$ , LUMO =  $-2.41 \text{ eV}$ ].<sup>[13]</sup> The attachment of BMes<sub>2</sub> to the ppy chelate leads to the decrease of both LUMO and HOMO levels (Figure 6). However, the decrease of the LUMO level of Pt(BppyB)(acac) is much more pronounced than that of **1**, thus supporting

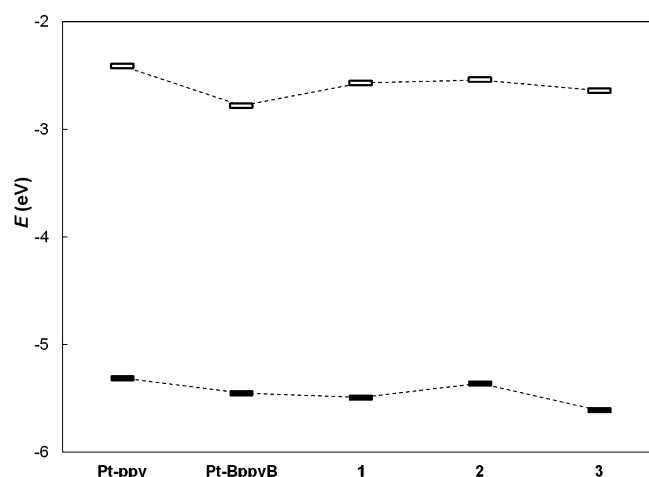


Figure 6. Comparison of experimental HOMO and LUMO energy levels of **1–3** with Pt(ppy)(acac) and Pt(BppyB)(acac).

that BMes<sub>2</sub> substitution at the 4'-position of the phenyl ring is much better for achieving high phosphorescence energy.

Among compounds **1–3**, the electron-withdrawing fluoro group significantly stabilizes the HOMO level and the LUMO level as well in **3**, albeit to less a degree, leading to the highest emission energy. In contrast, the electron-donating methyl group in **2** destabilizes the HOMO level but does not change the LUMO level significantly, resulting in the lowest emission energy among the three compounds. The influence of the fluoro and the methyl group on HOMO and LUMO energies may be attributed to the electronic induction effect. These data support that the introduction of a BMes<sub>2</sub> group at the 4'-position of the ppy ligand is an effective approach in shifting the emission energy of phosphorescent Pt<sup>II</sup> compounds toward blue.

For compound **4**, the reduction potential is at  $-2.09 \text{ V}$ , slightly more positive than that<sup>[14]</sup> of the non-borylated Pt(dpb)Cl ( $-2.14 \text{ V}$ ). Because the HOMO–LUMO gaps of **4** and Pt(dpb)Cl are similar, the addition of the BMes<sub>2</sub> group to the N,C,N-chelate must decrease both the LUMO and the HOMO level, thus maintaining the same HOMO–LUMO gap.

To further understand the photophysical properties of these materials, we have examined their electronic structures in detail using TD-DFT calculations.<sup>[16]</sup> Molecular orbital and molecular geometry calculations were performed by using the Gaussian 03 program suite with crystal struc-

Table 3. Experimental data of HOMO/LUMO energy and DFT calculation results.

Complex	Experimental			DFT results				
	HOMO [eV] <sup>[a]</sup>	LUMO [eV] <sup>[b]</sup>	$E_g$ [eV]	HOMO [eV] <sup>[c]</sup>	LUMO [eV] <sup>[c]</sup>	HOMO–LUMO gap [eV]	% HOMO→LUMO ( $S_0 \rightarrow S_1$ )	Oscillator strength ( $S_0 \rightarrow S_1$ )
<b>1</b>	−5.49	−2.57	2.92	−5.54	−1.67	3.87	78	0.0414
<b>2</b>	−5.36	−2.54	2.82	−5.42	−1.64	3.78	79	0.0314
<b>3</b>	−5.61	−2.64	2.97	−5.62	−1.73	3.89	85	0.0239
<b>4</b>	−5.60	−2.82	2.78	−5.56	−1.98	3.58	86	0.0283

[a] Calculated by using the reduction potential and the optical energy gap ( $E_g$ );  $E_g$  was determined from absorption edge. [b] Estimated by using the reduction potential. [c] HOMO and LUMO energies were determined by DFT calculation.

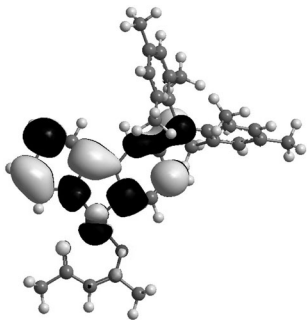
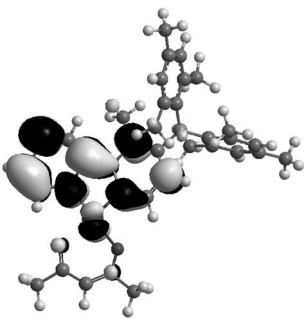
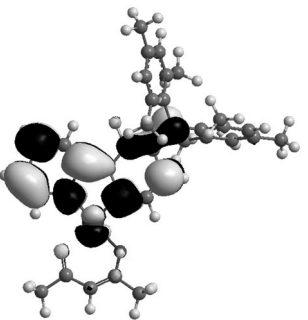
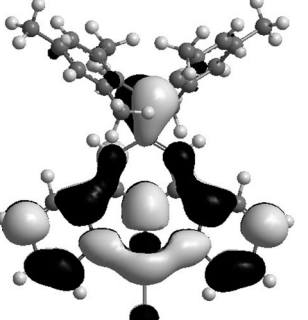
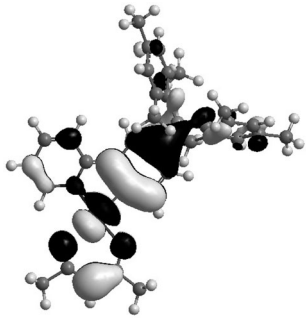
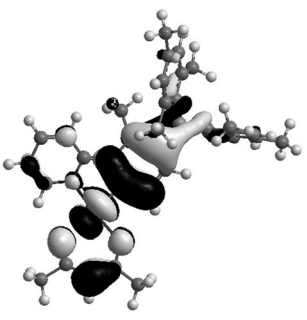
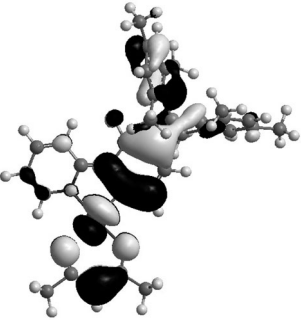
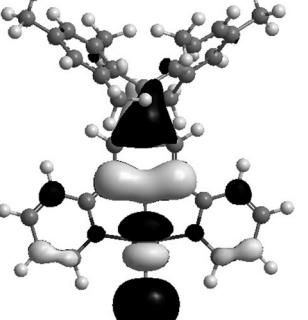
tures as the starting point for geometry optimizations where possible. Calculations were performed at the B3LYP level of theory by using LAN2LDZ as the basis set for Pt, and 6-31G\* for all other atoms. The computational results show that the  $S_0 \rightarrow S_1$  transitions arise predominantly from the HOMO and LUMO with reasonable oscillator strengths (Table 3). Hence, our discussion will focus on these orbitals (Table 4). The trends in the calculated and observed energy gaps are in reasonably good agreement. The HOMO levels of **1–3** have significant contributions from the d orbital of the Pt atom, some minor contributions from the acac ligand and major contributions from the phenyl ring of the ppy chelate. It should be noted that there is a large contribution by the carbon atom at the 4' (*para* to Pt) position of the phenyl ring at the HOMO level. In contrast, at the LUMO level, the contribution from the 4'-carbon atom is very small. Thus, substitution by an electron-withdrawing BMes<sub>2</sub> group at this position should be very effective in stabilizing the HOMO level through both induction effect and  $\pi$  conjugation while minimizing the impact on the LUMO level. This explains the observed increase of the HOMO–LUMO gap and emission energy of compounds **1–3**, compared to Pt(ppy)(acac). In contrast, the impact of BMes<sub>2</sub> substitution at the 5'-position of the phenyl ring to the HOMO level is much less due to the small orbital/electron density contribution at the 5'-position whereas the LUMO level can be significantly stabilized by the Boron center due to the large contribution at the 5'-position in the LUMO level. This ex-

plains the observed decrease of the HOMO–LUMO gap and the emission energy of Pt(BppyB)(acac), compared to Pt(ppy)(acac) (Figure 6).

For **4**, the LUMO level is dominated by the empty p orbital of the boron atom and the  $\pi^*$  orbital of the N,C,N-chelate, whereas the HOMO level has major contributions from the central benzene ring, the Pt atom and the chloro ligand. Thus, the electronic transition of the first excited state of compound **4** may be considered as a mixture of intraligand charge transfer, metal-to-ligand charge transfer and  $\pi$ -to- $\pi^*$  transition of the chelate ligand. The carbon atom at the 4'-position of the benzene ring in **4** has a very large contribution to the HOMO level but has no contributions at all to the LUMO level. The influence of the BMes<sub>2</sub> group to the LUMO level is therefore limited to induction effect. It can, however, effectively stabilize the HOMO level through both induction effect and  $\pi$ -orbital overlap with the carbon atom at 4'-position of the benzene ring. Based on this analysis, the slight widening of the HOMO–LUMO gap in **4** relative to that of Pt(dpb)Cl is caused mainly by the stabilization of the HOMO level through the boron atom.

**Electroluminescence:** Complexes **1**, **3** and **4** were selected for evaluation of performance in electroluminescent devices due to their relatively high emission energy and phosphorescence efficiency. The devices we fabricated have a double-layer structure with CBP (4,4'-N,N'-dicarbazolebiphenyl) as hole-transport layer (HTL) and host and 1,3,5-tris(N-phe-

Table 4. The surfaces and energies of frontier orbitals for **1–4** plotted with an isocontour value of 0.02.

	1	2	3	4
LUMO	 –1.67 eV	 –1.64 eV	 –1.73 eV	 –1.98 eV
HOMO	 –5.54 eV	 –5.42 eV	 –5.62 eV	 –5.56 eV

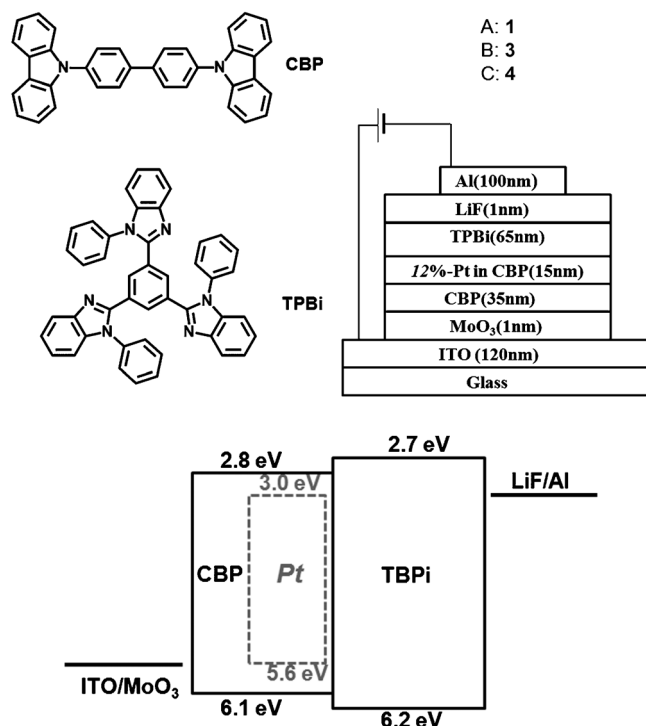


Figure 7. EL device structure (top) and energy level diagrams (bottom).

nylbenzimidazole-2-yl)benzene (TPBi) as the electron-transport layer (ETL) as shown in Figure 7. This device structure has been used successfully recently for green Pt<sup>II</sup> phosphorescent emitters by our group.<sup>[7c]</sup> Previously we have shown that a transition metal oxide hole injection layer, such as MoO<sub>3</sub>, raises the work function of the ITO anode sufficiently so as to allow direct charge injection into the host material, eliminating the need for a discrete HTL entirely.<sup>[17]</sup> Using the double-layer device structure design, we made a series of EL devices by varying the doping level of the Pt<sup>II</sup> compound in the CBP layer at 2, 4, 8 and 12%. No excimer emission was observed for any of the devices. For compounds **3** and **4** the best performance was achieved at a doping level of 12% whereas for **1** the best performance was observed at a doping level of 8%. For comparison purpose, the performance of EL devices at the 12% doping level for all three emitters are summarized in Table 5. The data for devices at 2, 4 and 8% doping levels for all three compounds can be found in the Supporting Information. The EL spectra of these devices ( $\lambda_{\text{max}} = 483$  nm for device A,

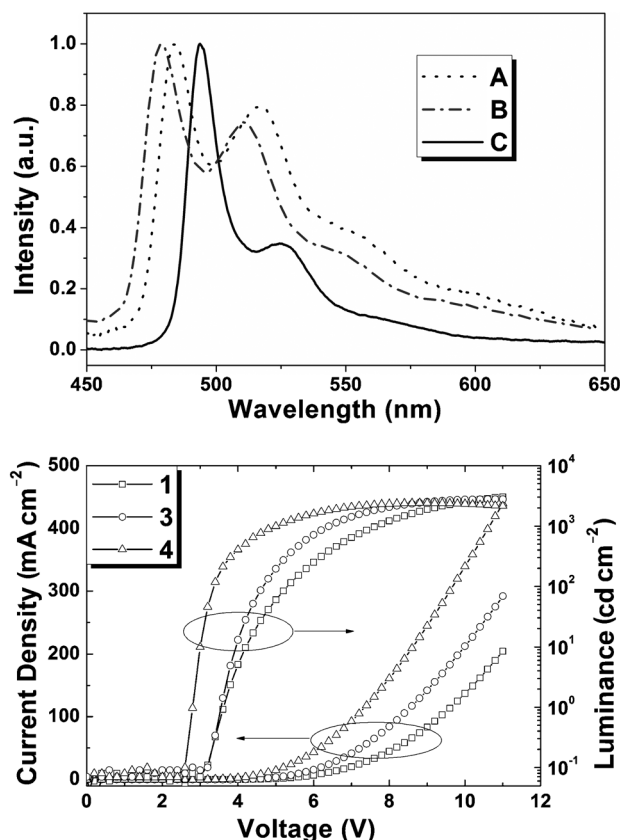


Figure 8. Left: EL spectra of devices A, B and C. Right: The *J*-*L*-*V* characteristics of devices A, B and C by using Pt compounds **1**, **3**, and **4** as the phosphorescent dopant, respectively.

478 nm for B and 493 nm for C) are shown in Figure 8, which match very well with the PL spectra of compounds **1**, **3** and **4**.

As shown in Figure 9, the EL devices based on compounds **1**, **3** and **4** have an impressive performance. For **1** and **3**, the turn-on voltage of the devices is about 3.5 V whereas for **4** it is 2.8 V with maximum brightness reaching 3025 cd m<sup>-2</sup> and 2765 cd m<sup>-2</sup>, respectively. At the 12% doping level, the external quantum efficiencies of devices **1** and **3** at 100 cd m<sup>-2</sup> are 4.7 and 6.5%, respectively. At the 8% doping level, the EQE of the EL device of **1** is 5.7% at 100 cd m<sup>-2</sup> with a maximum brightness of 3340 cd m<sup>-2</sup>. Although the device efficiencies of **1** and **3** are lower than the green PhOLEDs based on Pt(BppyA)(acac) we reported previously,<sup>[6a,c]</sup> it is certainly among the most efficient

Table 5. OLEDs characteristics for **1**, **3** and **4** at 12 wt % doping level.

12 wt % dopant	$V_{\text{on}}$ [V] <sup>[a]</sup>	$L$ [cd m <sup>-2</sup> ], [V] <sup>[b]</sup>	$\eta_{\text{ext}}$ [%] <sup>[c]</sup>			$\eta_e$ [cd A <sup>-1</sup> ] <sup>[d]</sup>	$\eta_p$ [lm W <sup>-1</sup> ] <sup>[d]</sup>	CIE (x,y)
			10 cd m <sup>-2</sup>	100 cd m <sup>-2</sup>	1000 cd m <sup>-2</sup>			
<b>1</b>	3.6	3025, 11.0	5.1	4.7	3.5	8.9	8.7	(0.33, 0.34)
<b>3</b>	3.5	2765, 10.5	6.7	6.5	4.5	16.5	16.2	(0.28, 0.44)
<b>4</b>	2.8	2417, 9.0	15.3	13.4	3.6	30.1	33.8	(0.34, 0.56)

[a] The applied voltage ( $V_{\text{on}}$ ) is defined as brightness of 1 cd m<sup>-2</sup>. [b] The luminance ( $L$ ) is maximum value. [c] External quantum efficiency (EQE,  $\eta_{\text{ext}}$ ). [d] Current efficiency ( $\eta_e$ ) and power efficiency ( $\eta_p$ ) are maximum values.



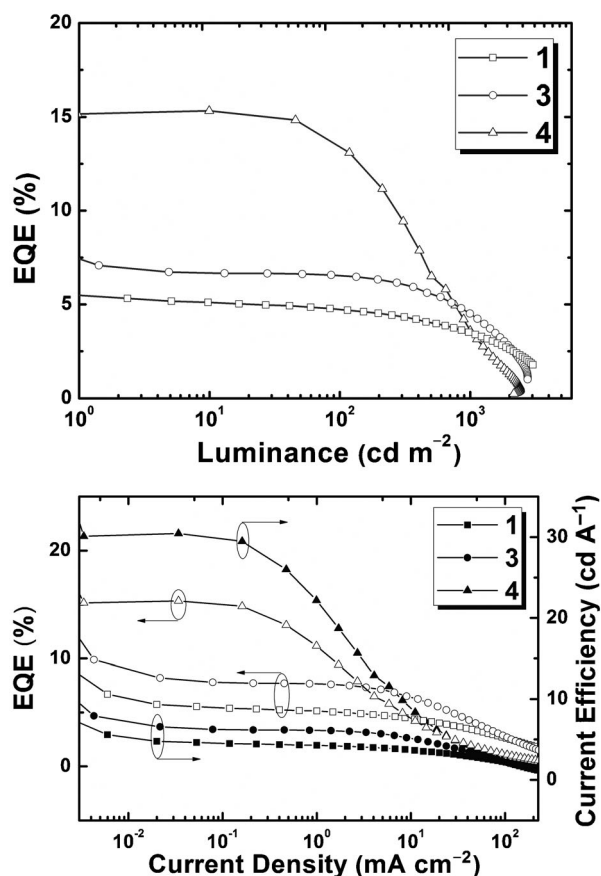


Figure 9. The external quantum efficiencies of EL devices versus luminance (top) and current density (bottom).

bluish-green PhOLEDs based on Pt(acac) compounds.<sup>[4c,8]</sup> The relatively low external quantum efficiencies of EL devices of **1** and **3** can be attributed to the relatively low photoluminescent quantum efficiencies of **1** and **3**, compared to that of Pt(BppyA)(acac) (0.98 in CH<sub>2</sub>Cl<sub>2</sub>). In fact, if we take the photoluminescent quantum efficiency (0.25 in CH<sub>2</sub>Cl<sub>2</sub>) of **3** into consideration, the EQE of EL device **3** is close to the commonly accepted theoretical limit for typical OLEDs.<sup>[18]</sup> Most significant is that the EL devices based on **1** and **3** maintain the high efficiency at high brightness and high current density and show little tendency of high current “roll-off” often observed in OLEDs.

The EL devices based on compound **4** have the most impressive performance (Figure 9 and Table 5). At the 12% doping level, the EQE of device C is 15.3% at 10 cd m<sup>-2</sup> luminance and 13.4 cd m<sup>-2</sup> at 100 cd m<sup>-2</sup> luminance with a brightness of 2417 cd m<sup>-2</sup> at 9 V. At the 8% doping level, the device performance remains impressive with EQE of 16.1% at 10 cd m<sup>-2</sup> luminance and 10.6 cd m<sup>-2</sup> at 100 cd m<sup>-2</sup> luminance, respectively, and a brightness of 2242 cd m<sup>-2</sup> at 9.2 V. Efficient blue-green and green PhOLEDs based on Pt(dpb)Cl and its derivatives have been demonstrated previously by Williams and colleagues, and others.<sup>[9]</sup> Compared to the previously reported Pt-N,C,N compounds-doped EL devices, the performance of the EL devices based on com-

pound **4** is certainly much better in terms of device efficiency, thus demonstrating that the BMes<sub>2</sub> group is also highly effective in enhancing the performance of N,C,N-chelate Pt<sup>II</sup> compounds.

## Conclusion

We have demonstrated that substitution by a BMes<sub>2</sub> group in a ppy chelate ligand is a highly effective strategy to enhance the phosphorescent efficiency of the corresponding Pt(acac) compounds. The location of the BMes<sub>2</sub> group on the ppy has a dramatic impact on the phosphorescent energy. Substitution at the 4'-position of the phenyl ring of ppy by BMes<sub>2</sub> has been found to effectively shift the phosphorescent emission energy of the Pt<sup>II</sup> compound to the blue-green region, which can be further tuned by a substituent at the 3'-position. BMes<sub>2</sub> substitution on the dipyrityl-benzene N,C,N-chelate ligand does not significantly change the phosphorescent energy of the Pt<sup>II</sup> compound, it does, however, increase phosphorescent quantum efficiency, minimize excimer emission and greatly enhance the performance of the EL devices. High performance bluish-green EL devices with a simple double-layer structure and compounds **1**, **3** and **4** as the dopants have been achieved, demonstrating once again the important role played by the BMes<sub>2</sub> group in achieving high efficiency PhOLEDs.

## Experimental Section

**General consideration and measurement:** All experiments were carried out under a dry nitrogen atmosphere by using standard Schlenk techniques. All starting materials were purchased from either Aldrich Chemical Co. or Strem Chemicals, Inc., and used without further purification. <sup>1</sup>H and <sup>13</sup>C NMR spectra were recorded on a Bruker Avance 300 or 400 MHz spectrometer. UV/Vis spectra were obtained on a Varian Cary 50 UV/Vis spectrophotometer with all sample concentrations in the range 10–50 μM. Excitation and emission spectra were recorded on a Photon Technologies International QuantaMaster Model 2 spectrometer. Photoluminescent lifetimes were measured on a Photon Technology International Phosphorescent lifetime spectrometer, Timemaster C-631F equipped with a xenon flash lamp and digital emission photon multiplier tube for both excitation and emission. All solutions for photophysical experiments were degassed with nitrogen. Phosphorescence quantum yields of complexes **1** to **4** were obtained relative to Ir(ppy)<sub>3</sub> in degassed CH<sub>2</sub>Cl<sub>2</sub> (Φ<sub>PL</sub> = 1.0)<sup>[19]</sup> at 298 K, and calculated by using previously reported procedures.<sup>[20]</sup> Cyclic voltammetry was performed by using a BAS CV-50W voltammetric analyzer with scan rates of either 50 or 100 mV s<sup>-1</sup>. The electrolytic cell used was a conventional three compartment cell, with a Pt working electrode, Pt wire auxiliary electrode, and Ag/AgCl reference electrode. All experiments were performed at room temperature by using NBu<sub>4</sub>PF<sub>6</sub> (0.10 M) in DMF as the supporting electrolyte. The ferrocenium/ferrocene couple (E<sub>onset</sub> = 0.55 V) was used as the internal standard. The starting materials, (3-bromophenyl)dimesitylborane and 2-(2'-(dimesitylboryl)phenyl)pyridine (Bppy) were synthesized according to a literature procedure.<sup>[10]</sup> TD-DFT computations were performed by using Gaussian 03 software<sup>[16]</sup> and the High Performance Computing Virtual Laboratory (HPCVL) at Queen's University.

### Synthesis of ligands

2-(5'-(Dimesitylboryl)-6'-fluorophenyl)pyridine (Bfppy): *n*-Butyllithium (0.63 mL, 1.60 M in hexanes, 1.00 mmol) was slowly added to a solution of

2-(2-fluoro-3-bromophenyl)pyridine (0.25 g, 1.00 mmol) in THF at  $-78^{\circ}\text{C}$ . The solution was then stirred for 1 h at  $-78^{\circ}\text{C}$  before  $\text{BMe}_2\text{F}$  (0.30 g, 1.10 mmol) was added. The resulting solution was maintained at  $-78^{\circ}\text{C}$  for an additional hour, then slowly warmed to room temperature and stirred, overnight. The concentration of the solution under vacuum and further purification by chromatography on silica gel afforded the desired product in 80% yield.  $^1\text{H}$  NMR (400 MHz,  $\text{CD}_2\text{Cl}_2$ ,  $25^{\circ}\text{C}$ , TMS):  $\delta$  = 8.76 (d,  $^3J$  = 4.5 Hz, 1H), 8.19 (t,  $^3J$  = 8.0 Hz, 1H), 7.79 (d,  $^3J$  = 8.5 Hz, 1H), 7.68 (t,  $^3J$  = 7.0 Hz, 1H), 7.39 (t,  $^3J$  = 7.0 Hz, 1H), 7.32 (t,  $^3J$  = 7.5 Hz, 1H), 7.23 (t,  $^3J$  = 6.0 Hz, 1H), 6.80 (s, 4H), 2.36 (s, 6H), 2.16 ppm (s, 12H).

**2-Bromo-6-dimesitylboryltoluene:** A solution of *n*-butyllithium (6.00 mL, 1.60 M solution in hexane, 9.6 mmol) was added dropwise to a solution of 2,6-dibromotoluene (2.00 g, 8.00 mmol) in  $\text{Et}_2\text{O}$  (30 mL) at  $-78^{\circ}\text{C}$ . The reaction mixture was maintained at this temperature for an additional hour, and then  $\text{BMe}_2\text{F}$  (2.57 g, 9.60 mmol) in  $\text{Et}_2\text{O}$  (50 mL) was added slowly. The reaction mixture was allowed to warm to room temperature and stirred, overnight. The reaction mixture was quenched with water, and then extracted with  $\text{CH}_2\text{Cl}_2$ . The organic layers were combined and washed with water, dried over  $\text{MgSO}_4$ , and then filtered. The filtrate was concentrated under reduced pressure. The residue was purified by silica column chromatography by using hexane to give the product in 75% yield as a white solid.  $^1\text{H}$  NMR (300 MHz,  $\text{CDCl}_3$ ,  $25^{\circ}\text{C}$ , TMS):  $\delta$  = 7.63 (d,  $^3J$  = 7.8 Hz, 1H), 7.05–7.15 (m, 2H), 6.83 (s, 4H), 2.32 (s, 6H), 2.24 (s, 3H), 1.99 ppm (s, 12H).

**2-(5'-Dimesitylboryl-6'-methylphenyl)pyridine (Bmppy):** A Schlenk flask was charged with 2-bromopyridine (0.87 g, 5.50 mmol) and dry THF (15 mL). This solution was cooled to  $-78^{\circ}\text{C}$ , then *n*-butyllithium (4.1 mL, 1.60 M solution in hexane, 6.56 mmol) was added dropwise via syringe. The resulting solution was stirred at  $-78^{\circ}\text{C}$  for 1 h.  $\text{ZnCl}_2(\text{tmeda})$  (1.60 g, 6.60 mmol) in THF (66 mL) was added slowly at the same temperature via cannula. After 30 min at  $-78^{\circ}\text{C}$ , the reaction mixture was allowed to warm to room temperature and stirred for 1 h.  $\text{Pd}(\text{PPh}_3)_4$  (0.32 g, 5 mol%) and (3-bromo-2-methylphenyl)dimesitylborane (2.32 g, 5.5 mmol) in THF (20 mL) were added to the reaction mixture. The reaction mixture was refluxed, overnight, and then cooled to room temperature. All volatiles were removed under reduced pressure, and the residue was then extracted with  $\text{CH}_2\text{Cl}_2$ . Organic layers were combined and washed with water, dried over  $\text{MgSO}_4$ , and then filtered. The filtrate was concentrated under reduced pressure. The residue was purified by silica column chromatography by using ethylacetate/hexane (1:3 v/v) to give the product in 50% yield as a white solid.  $^1\text{H}$  NMR (300 MHz,  $\text{CDCl}_3$ ,  $25^{\circ}\text{C}$ , TMS):  $\delta$  = 8.68 (d,  $^4J$  = 3.9 Hz, 1H), 7.76 (td,  $^3J$  = 7.8 Hz,  $^4J$  = 1.8 Hz, 1H), 7.44 (dd,  $^3J$  = 6.0 Hz,  $^4J$  = 2.7 Hz, 1H), 7.38 (d,  $^3J$  = 7.8 Hz, 1H), 7.25 (m, 3H), 6.84 (s, 4H), 2.32 (s, 6H), 2.20 (s, 3H), 1.99 ppm (s, 12H).

**1-Dimesitylboryl-3,5-dibromobenzene:** A solution of *n*-butyllithium (2.0 mL; 1.60 M in hexanes, 3.20 mmol) was slowly added to a solution of 1,3,5-tribromobenzene (1.00 g, 3.20 mmol) in THF at  $-78^{\circ}\text{C}$ . The solution was then stirred for 1 h at  $-78^{\circ}\text{C}$  before  $\text{BMe}_2\text{F}$  (0.94 g, 3.50 mmol) was added. The resulting solution was maintained at  $-78^{\circ}\text{C}$  for an additional hour, then slowly warmed to room temperature and stirred, overnight. The concentration of the solution under vacuum and further purification by chromatography on silica gel gave a white solid. Recrystallization produced the product in 45% yield.  $^1\text{H}$  NMR (300 MHz,  $\text{CDCl}_3$ ,  $25^{\circ}\text{C}$ , TMS):  $\delta$  = 7.82 (t,  $^4J$  = 1.5 Hz, 1H), 7.53 (d,  $^4J$  = 1.5 Hz, 2H), 6.83 (s, 4H), 2.36 (s, 6H), 2.02 ppm (s, 12H).

**1-Dimesitylboryl-3,5-dipyridylbenzene (Bdppb):** Excess 2-(tributylstannyl)pyridine (1.82 mL, 4.80 mmol), LiCl (0.40 g, 9.50 mmol) and  $\text{Pd}(\text{PPh}_3)_4$  (0.055 g, 0.08 mmol) were added to the toluene solution of 1-dimesitylboryl-3,5-dibromobenzene (0.95 mmol). The solution was then stirred and refluxed for 3 days under nitrogen. Purification through column chromatography by using  $\text{CH}_2\text{Cl}_2$ /hexanes afforded a white solid of Bdppb (0.14 g, 30%).  $^1\text{H}$  NMR (300 MHz,  $\text{CD}_2\text{Cl}_2$ ,  $25^{\circ}\text{C}$ , TMS):  $\delta$  = 8.91 (s,  $^4J$  = 1.5 Hz, 1H), 8.72 (d,  $^3J$  = 3.5 Hz, 2H), 8.20 (d,  $^4J$  = 1.5 Hz, 2H), 7.80 (m, 4H), 7.29 (t,  $^4J$  = 1.5 Hz, 2H), 6.93 (s, 4H), 2.38 (s, 6H), 2.10 ppm (s, 12H).

**Synthesis of Pt(acac) compounds:**  $\text{BMe}_2$ -functionalized Pt(acac) compounds were synthesized by the general procedure similar to the one re-

ported recently for N,C-chelate Pt(acac) compounds.<sup>[12]</sup> A typical procedure is given below.

The starting material<sup>[21]</sup>  $[\text{PtMe}_2(\text{SMe}_2)]_2$  and corresponding  $\text{BMe}_2$ -functionalized phenylpyridine were dissolved in THF ( $\sim 5$  mL) and then this mixture was stirred for 1 h at ambient temperature. Trifluoromethanesulfonic acid ( $\text{TfOH}$ ) in THF was added slowly to this solution. After 30 min,  $\text{Na}(\text{acac})\cdot\text{H}_2\text{O}$  in methanol was added and stirred for 1 to 2 h. The pale yellow precipitate formed was filtered and washed with  $\text{Et}_2\text{O}$ . An analytically pure  $\text{BMe}_2$ -functionalized Pt(ppy)(acac) was isolated in the range of 80–90% yield.

**Synthesis of Pt-Bppy (1):** Yield: 92%;  $^1\text{H}$  NMR (400 MHz,  $\text{CD}_2\text{Cl}_2$ ,  $25^{\circ}\text{C}$ , TMS):  $\delta$  = 9.24 (d, sat,  $^3J$  = 5.6 Hz,  $J_{\text{Pt-H}}$  = 36 Hz, 1H), 7.81 (td,  $^3J$  = 8.0 Hz,  $^4J$  = 1.6 Hz, 1H), 7.65–7.53 (m, 3H), 7.28 (dd,  $^3J$  = 7.6 Hz,  $^4J$  = 1.2 Hz, 1H), 7.18 (td,  $^3J$  = 6.4 Hz,  $^4J$  = 1.2 Hz, 1H), 6.87 (s, 4H), 5.55 (s, 1H), 2.35 (s, 6H), 2.07 (s, 12H), 2.06 (s, 3H), 2.02 ppm (s, 3H);  $^{13}\text{C}$  NMR (100 MHz,  $\text{CD}_2\text{Cl}_2$ ,  $25^{\circ}\text{C}$ , TMS):  $\delta$  = 186.2, 184.4, 167.9, 147.9, 147.2, 144.9, 140.7, 138.2, 131.2, 130.3, 128.2, 128.1, 121.5, 118.6, 102.3, 27.9, 26.9, 23.2, 20.9 ppm; elemental analysis calcd (%) for  $\text{C}_{33}\text{H}_{35}\text{BNO}_2\text{Pt}$ : C 57.99, H 5.16, N 2.05; found: C 57.89, H 5.19, N 2.08.

**Synthesis of Pt-Bmppy (2):** Yield: 89%;  $^1\text{H}$  NMR (400 MHz,  $\text{CD}_2\text{Cl}_2$ ,  $25^{\circ}\text{C}$ , TMS):  $\delta$  = 9.10 (dd, sat,  $^3J$  = 5.6 Hz,  $^4J$  = 1.2 Hz,  $J_{\text{Pt-H}}$  = 42 Hz, 1H), 7.79–7.74 (m, 2H), 7.45 (d, sat,  $^3J$  = 7.7 Hz,  $J_{\text{Pt-H}}$  = 28 Hz, 1H), 7.05 (td,  $^3J$  = 7.2 Hz,  $^4J$  = 1.2 Hz, 1H), 6.84 (d,  $^3J$  = 7.6 Hz, 1H), 6.70 (s, 4H), 5.41 (s, 1H), 2.40 (s, 3H), 2.20 (s, 6H), 1.93 (s, 12H), 1.87 (s, 3H), 1.45 ppm (s, 3H);  $^{13}\text{C}$  NMR (100 MHz,  $\text{CD}_2\text{Cl}_2$ ,  $25^{\circ}\text{C}$ , TMS):  $\delta$  = 186.3, 184.4, 168.4, 147.8, 146.2, 143.8, 143.4, 140.2, 138.5, 137.9, 134.8, 128.2, 128.0, 123.2, 120.8, 102.2, 28.0, 26.9, 22.8, 20.9 ppm; elemental analysis calcd (%) for  $\text{C}_{34}\text{H}_{37}\text{BNO}_2\text{Pt}$ : C 58.54, H 5.35, N 2.01; found: C 58.52, H 5.38, N 2.05.

**Synthesis of Pt-Bfppy (3):** The Pt complex was synthesized the same way as indicated in the literature.<sup>[6a]</sup> Bright yellow crystals were obtained after recrystallization from DCM/hexane.  $^1\text{H}$  NMR (400 MHz,  $\text{CD}_2\text{Cl}_2$ ,  $25^{\circ}\text{C}$ , TMS):  $\delta$  = 9.11 (d,  $^4J$  = 0.5 Hz, 1H), 8.02 (d,  $^3J$  = 8.5 Hz, 1H), 7.86 (t,  $^3J$  = 8.0 Hz, 1H), 7.45 (d,  $^3J$  = 8.5 Hz, 1H), 7.20 (t,  $^3J$  = 7.5 Hz, 1H), 7.06 (t,  $^3J$  = 7.5 Hz, 1H), 6.85 (s, 4H), 5.54 (s, 1H), 2.33 (s, 6H), 2.10 (s, 12H), 1.75 (s, 3H), 1.15 ppm (s, 3H);  $^{13}\text{C}$  NMR (100 MHz,  $\text{CD}_2\text{Cl}_2$ ,  $25^{\circ}\text{C}$ , TMS):  $\delta$  = 186.4, 184.5, 147.4, 140.2, 138.8, 138.5, 137.6, 137.5, 128.1, 126.4, 123.4, 123.2, 121.6, 102.4, 27.9, 26.8, 22.8, 20.9 ppm; elemental analysis calcd (%) for  $\text{C}_{34}\text{H}_{35}\text{BFNO}_2\text{Pt}$ : C 57.15, H 4.94, N 1.96; found: C 56.97, H 4.95, N 1.87.

**Synthesis of Pt-(Bdppb)Cl (4):** Bdppb (0.029 g, 0.06 mmol) and  $\text{K}_2\text{PtCl}_4$  (0.028 g, 0.066 mmol) were stirred in degassed acetonitrile and water (3:1; 5 mL) mixture at  $90^{\circ}\text{C}$ , overnight. After removal of the solvent and further recrystallization from hexane/ $\text{CH}_2\text{Cl}_2$ , orange crystals of the complex **4** were obtained (0.04 g, 94%).  $^1\text{H}$  NMR (400 MHz,  $\text{CDCl}_3$ ,  $25^{\circ}\text{C}$ , TMS):  $\delta$  = 9.40 (d, sat,  $^4J$  = 1.0 Hz,  $J_{\text{Pt-H}}$  = 60 Hz, 1H), 7.92 (td,  $^3J$  = 10 Hz,  $^4J$  = 1.5 Hz, 2H), 7.65 (d,  $^3J$  = 10 Hz, 2H), 7.61 (s, 2H), 7.31 (td,  $^3J$  = 8.0 Hz,  $^4J$  = 1.5 Hz, 2H), 6.87 (s, 4H), 2.36 (s, 6H), 2.07 ppm (s, 12H);  $^{13}\text{C}$  NMR (100 MHz,  $\text{CDCl}_3$ ,  $25^{\circ}\text{C}$ , TMS):  $\delta$  = 168.4, 167.2, 152.2, 141.6, 141.0, 140.8, 139.2, 138.7, 132.5, 128.3, 123.2, 119.6, 23.6, 21.3 ppm; elemental analysis calcd (%) for  $\text{C}_{34}\text{H}_{32}\text{BClN}_2\text{Pt}$ : C 57.52, H 4.54, N 3.95; found: C 57.02, H 4.37, N 3.85.

**EL device fabrication:** Devices were fabricated in a Kurt J. Lesker LU-MINOS® cluster tool with a base pressure of approximately  $10^{-8}$  Torr without breaking vacuum. The ITO anode is commercially patterned and coated on glass substrates  $50 \times 50 \text{ mm}^2$  with a sheet resistance less than  $15 \Omega$ . Substrates were ultrasonically cleaned with a standard regiment of Alconox®, acetone, and methanol followed by UV ozone treatment for 15 min. The active area for all devices was  $2 \text{ mm}^2$ . The film thicknesses were monitored by a calibrated quartz crystal microbalance and were further verified for single-carrier devices by using capacitance-voltage measurements (Agilent 4294A). *I*-*V* characteristics were measured by using a HP4140B picoammeter in ambient air. Luminance measurements and EL spectra were taken by using a Minolta LS-110 luminance meter and an Ocean Optics USB200 spectrometer with bare fiber, respectively. The external quantum efficiency of EL devices was calculated following the standard procedure.<sup>[22]</sup> After deposition, single carrier devices were transferred to a homebuilt variable temperature cryostat for measurement at

298 K. Additional details regarding device fabrication, and characterization have been described elsewhere.<sup>[23]</sup>

**X-ray crystallography analysis:** Single crystals of **1**, **2**, **3** and **4** were mounted on glass fibers and were collected on a Bruker Apex II single-crystal X-ray diffractometer with graphite-monochromated Mo<sub>Kα</sub> radiation, operating at 50 kV and 30 mA and at 180 K. Data were processed on a PC with the aid of the Bruker SHELXTL software package (version 6.14)<sup>[24]</sup> and corrected for absorption effects. All non-hydrogen atoms were refined anisotropically. Complete crystal structural data can be found in the Supporting Information. CCDC 875462 (**1**), 875463 (**2**), 875464 (**4**) and 875465 (**3**) contain the supplementary crystallographic data for this paper. These data can be obtained free of charge from The Cambridge Crystallographic Data Centre via [www.ccdc.cam.ac.uk/data\\_request/cif](http://www.ccdc.cam.ac.uk/data_request/cif).

## Acknowledgements

We thank the Natural Sciences and Engineering Research Council of Canada for financial support.

- [1] a) M. A. Baldo, D. F. O'Brien, Y. You, A. Shoustikov, S. Sibley, M. E. Thompson, S. R. Forrest, *Nature* **1998**, 395, 151; b) L. Xiao, Z. Chen, B. Qu, J. Luo, S. Kong, Q. Gong, J. Kido, *Adv. Mater.* **2011**, 23, 926, and references therein; c) F. So, J. Kido, P. Burrows, *MRS Bull.* **2008**, 33, 663; d) P.-T. Chou, Y. Chi, *Chem. Eur. J.* **2007**, 13, 380.
- [2] a) S.-J. Su, E. Gonmori, H. Sasabe, J. Kido, *Adv. Mater.* **2008**, 20, 4189; b) R. J. Holmes, S. R. Forrest, Y.-J. Tung, R. C. Kwong, J. J. Brown, S. Garon, M. E. Thompson, *Appl. Phys. Lett.* **2003**, 82, 2422; c) Y. Zheng, S.-H. Eom, N. Chopra, J. Lee, F. So, J. Xue, *Appl. Phys. Lett.* **2008**, 92, 223301; d) R. Ragni, E. A. Plummer, K. Brunner, J. W. Hofstra, F. Babudri, G. M. Farinola, F. Naso, L. De Cola, *J. Mater. Chem.* **2006**, 16, 1161; e) M. Xu, R. Zhou, G. Wang, Q. Xiao, W. Du, G. Che, *Inorg. Chim. Acta* **2008**, 361, 2407; f) J. Li, P. I. Djurovich, B. D. Alleyne, M. Yousufuddin, N. N. Ho, J. C. Thomas, J. C. Peters, R. Bau, M. E. Thompson, *Inorg. Chem.* **2005**, 44, 1713.
- [3] a) X. Ren, J. Li, R. J. Holmes, P. I. Djurovich, S. R. Forrest, M. E. Thompson, *Chem. Mater.* **2004**, 16, 4743; b) P.-T. Chou, Y. Chi, M.-W. Chung, C.-C. Lin, *Coord. Chem. Rev.* **2011**, 255, 2653; c) C.-H. Hsieh, F.-I. Wu, C.-H. Fan, M.-J. Huang, K.-Y. Lu, P.-Y. Chou, Y.-H. O. Yang, S.-H. Wu, I.-C. Chen, S.-H. Chou, K.-T. Wong, C.-H. Cheng, *Chem. Eur. J.* **2011**, 17, 9180; d) Y. Chi, P.-T. Chou, *Chem. Soc. Rev.* **2010**, 39, 638; e) Y. You, S. Y. Park, *Dalton Trans.* **2009**, 1267.
- [4] a) A. F. Rausch, H. H. H. Homeier, P. I. Djurovich, M. E. Thompson, H. Yersin, *Proc. SPIE-Int. Soc. Opt. Eng.* **2007**, 6655, 66550F/1; b) B. Ma, P. I. Djurovich, S. Garon, B. Alleyne, M. E. Thompson, *Adv. Funct. Mater.* **2006**, 16, 2438; c) V. Adamovich, J. Brooks, A. Tamayo, A. M. Alexander, P. I. Djurovich, B. W. D'Andrade, C. Adachi, S. R. Forrest, M. E. Thompson, *New J. Chem.* **2002**, 26, 1171; d) B. W. D'Andrade, J. Brooks, V. Adamovich, M. E. Thompson, S. R. Forrest, *Adv. Mater.* **2002**, 14, 1032; e) J. A. G. Williams, S. Develay, D. L. Rochester, L. Murphy, *Coord. Chem. Rev.* **2008**, 252, 2596.
- [5] H. L. Schläfer, G. Gliemann, *Basic Principles of Ligand Field Theory*, Wiley, New York, **1969**.
- [6] a) W. Y. Wong, Z. He, S.-K. So, K.-L. Tong, Z. Lin, *Organometallics* **2005**, 24, 4079; b) G. Zhou, Q. i. Wang, X. Wang, C.-L. Ho, W.-Y. Wong, D. Ma, L. Wang, Z. Lin, *J. Mater. Chem.* **2010**, 20, 7472; c) J. Kavitha, S.-Y. Chang, Y. Chi, J.-K. Yu, Y.-H. Hu, P.-T. Chou, S.-M. Peng, G.-H. Lee, Y.-T. Tao, C.-H. Chien, A. J. Carty, *Adv. Funct. Mater.* **2005**, 15, 223; d) S.-Y. Chang, J. Kavitha, J.-Y. Hung, Y. Chi, Y.-M. Cheng, E. Y. Li, P.-T. Chou, G.-H. Lee, A. J. Carty, *Inorg. Chem.* **2007**, 46, 7064; e) S.-Y. Chang, Y.-M. Cheng, Y. Chi, Y.-C. Lin, C.-M. Jiang, G.-H. Lee, P.-T. Chou, *Dalton Trans.* **2008**, 6901.
- [7] a) Z. M. Hudson, C. Sun, M. G. Helander, H. Amarné, Z.-H. Lu, S. Wang, *Adv. Funct. Mater.* **2010**, 20, 3426; b) Z. M. Hudson, S. Wang, *Dalton Trans.* **2011**, 40, 7805; c) Z. Wang, M. G. Helander, Z. M. Hudson, J. Qiu, S. Wang, Z.-H. Lu, *Appl. Phys. Lett.* **2011**, 98, 213301; d) Z. M. Hudson, M. G. Helander, Z.-H. Lu, S. Wang, *Chem. Commun.* **2011**, 47, 755.
- [8] a) K. Li, X. Guan, C.-W. Ma, W. Lu, Y. Chen, C.-M. Che, *Chem. Commun.* **2011**, 47, 9075; b) Y. Unger, D. Meyer, O. Molt, C. Schildknecht, I. Münster, G. Wagenblast, T. Strassner, *Angew. Chem.* **2010**, 122, 10412; *Angew. Chem. Int. Ed.* **2010**, 49, 10214; c) E. L. Williams, K. Madakuni, J. Li, G. E. Jabbour, *Adv. Mater.* **2007**, 19, 197.
- [9] a) M. Cocchi, J. Kalinowski, V. Fattori, J. A. G. Williams, L. Murphy, *Appl. Phys. Lett.* **2009**, 94, 073309; b) M. Cocchi, D. Virgili, V. Fattori, D. L. Rochester, J. A. G. Williams, *Adv. Funct. Mater.* **2007**, 17, 285; c) X. Yang, Z. Wang, S. Madakuni, J. Li, G. E. Jabbour, *Adv. Mater.* **2008**, 20, 2405; d) S.-Y. Chang, J.-L. Chen, Y. Chi, Y.-M. Cheng, G.-H. Lee, C.-M. Jiang, P.-T. Chou, *Inorg. Chem.* **2007**, 46, 11202.
- [10] Y. You, S. Y. Park, *Adv. Mater.* **2008**, 20, 3820.
- [11] G. J. Zhou, C. L. Ho, W. Y. Wong, Q. Wang, D. G. Ma, L. X. Wang, Z. Y. Lin, T. B. Marder, A. Beeby, *Adv. Funct. Mater.* **2008**, 18, 499.
- [12] Z. M. Hudson, B. A. Blight, S. Wang, *Org. Lett.* **2012**, 14, 1700.
- [13] J. Brooks, Y. Babayan, S. Lamansky, P. I. Djurovich, I. Tsyba, R. Bau, M. E. Thompson, *Inorg. Chem.* **2002**, 41, 3055.
- [14] J. A. G. Williams, A. Beeby, E. S. Davies, J. A. Weinstein, C. Wilson, *Inorg. Chem.* **2003**, 42, 8609.
- [15] Z. Wang, E. Turner, V. Mahoney, S. Madakuni, T. Groy, J. Li, *Inorg. Chem.* **2010**, 49, 11276.
- [16] M. J. Frisch, G. W. Trucks, H. B. Schlegel, G. E. Scuseria, M. A. Robb, J. R. Cheeseman, J. A. Montgomery, Jr., T. Vreven, K. N. Kudin, J. C. Burant, J. M. Millam, S. S. Iyengar, J. Tomasi, V. Barone, B. Mennucci, M. Cossi, G. Scalmani, N. Rega, G. A. Petersson, H. Nakatsuji, M. Hada, M. Ehara, K. Toyota, R. Fukuda, J. Hasegawa et al., *Gaussian 03*, Revision C.02, Gaussian, Inc., Wallingford, CT **2004**.
- [17] Z. B. Wang, M. G. Helander, J. Qiu, Z. W. Liu, M. T. Greiner, Z. H. Lu, *J. Appl. Phys.* **2010**, 108, 024510.
- [18] a) C. Adachi, M. A. Baldo, D. F. O'Brien, M. E. Thompson, S. R. Forrest, *J. Appl. Phys.* **2001**, 90, 5048; b) S.-J. Su, D. Tanaka, Y.-J. Li, H. Sasabe, T. Takeda, J. Kido, *Org. Lett.* **2008**, 10, 941; c) L. Xiao, S.-J. Su, Y. Agata, H. Lan, J. Kido, *Adv. Mater.* **2009**, 21, 1271.
- [19] T. Sajoto, P. I. Djurovich, A. B. Tamayo, J. Oxgaard, W. A. Goddard III, M. E. Thompson, *J. Am. Chem. Soc.* **2009**, 131, 9813.
- [20] a) S. J. Strickler, R. A. Berg, *J. Chem. Phys.* **1962**, 37, 814; b) E. M. Kober, J. L. Marshall, W. J. Dressick, B. P. Sullivan, J. V. Caspar, T. J. Meyer, *Inorg. Chem.* **1985**, 24, 2755.
- [21] G. S. Hill, M. J. Irwin, C. J. Levy, L. M. Rendina, R. J. Puddephatt, *Inorg. Synth.* **1998**, 32, 149.
- [22] S. R. Forrest, D. D. C. Bradley, M. E. Thompson, *Adv. Mater.* **2003**, 15, 1043.
- [23] a) M. G. Helander, M. T. Greiner, Z. B. Wang, Z. H. Lu, *Appl. Surf. Sci.* **2010**, 256, 2602; b) M. G. Helander, Z. B. Wang, M. T. Greiner, J. Qiu, Z. H. Lu, *Rev. Sci. Instrum.* **2009**, 80, 033901.
- [24] Shelxtl Version 6.14, Bruker AXS, copyright 2000–2003.

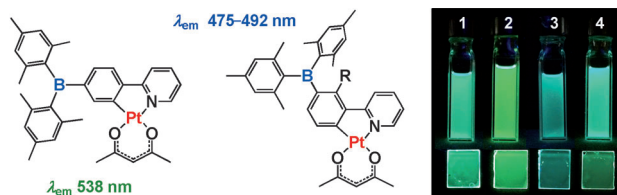
Received: April 13, 2012  
Published online: ■■■■, 0000

**Platinum**

Y.-L. Rao, D. Schoenmakers,  
Y.-L. Chang, J.-S. Lu, Z.-H. Lu,  
Y. Kang,\* S. Wang\* ..... ■■■■–■■■■



**Bluish-Green BMes<sub>2</sub>-Functionalized Pt<sup>II</sup> Complexes for High Efficiency PhOLEDs: Impact of the BMes<sub>2</sub> Location on Emission Color**



**Easily PhOLED:** Blue-green phosphorescent organic light-emitting diodes (PhOLEDs) based on BMes<sub>2</sub>-functionalized N,C-chelate and N,C,N-chelate Pt<sup>II</sup> compounds with external quantum efficiencies of 5 to 22 % have

been achieved (see figure). BMes<sub>2</sub> substitution and its location on the N,C- or N,C,N-chelate ligand have been found to be critical in achieving efficient blue-green phosphorescent Pt<sup>II</sup> compounds.